

# **Tunable band-selective photodetector based on sputter-deposited SnO<sub>x</sub> thin-films: Effect of reactive gas pulsing process**

F. Djeffal<sup>1,\*</sup>, N. Martin<sup>2</sup>, H. Ferhati<sup>1,3</sup> and A. Benhaya<sup>1</sup>

<sup>1</sup> LEA, Department of Electronics, University of Batna 2, Batna 05000, Algeria

<sup>2</sup> SUPMICROTECH, CNRS, Institut FEMTO-ST, 15B, Avenue des montboucons 25030 BESANCON Cedex, France

<sup>3</sup> ISTA, University of Larbi Ben M'hidi, Oum El Bouaghi, Algeria

\*E-mail: faycal.djeffal@univ-batna2.dz

## **Abstract**

In this work, high-performance SnO<sub>x</sub> band-selective photodetectors (PDs) were realized by DC magnetron sputtering technique. The reactive gas pulsing process (RGPP) was implemented with pulsing period fixed at  $P = 20$  s to adjust tin and oxygen concentrations in the film. The impact of pulsed oxygen time on the structural, morphological and photosensing properties of SnO<sub>x</sub>-based PDs was investigated. The fabricated SnO<sub>x</sub>-based PD at a high duty cycle of 80% of  $P$  demonstrated high UV photodetection capabilities and solar-blind characteristic with a high responsivity of 21.8 mA/W, a high signal to noise ratio of  $6 \times 10^4$  and a specific detectivity of about  $5 \times 10^{11}$  Jones. It was also revealed that the use of a short oxygen pulsing time 8 s paves the way for the realization of multispectral SnO<sub>x</sub> PD, demonstrating a high responsivity values of 36.45 mA/W, 36.4 mA/W and 34 mA/W over UV, Visible and NIR bands, respectively. This is attributed to the role of using RGPP in modulating the film optoelectronic properties from metallic to insulator when the duty cycle and thus oxygen concentration in the films changed from pure tin to overstoichiometric SnO<sub>2</sub> compound. The prepared SnO<sub>x</sub> PDs demonstrated many advantageous features like low-noise, cost effective and high sensitivity. The obtained results proved that SnO<sub>x</sub> can be used as an alternative material for developing high-performance band-selective sensing devices.

**Keywords:** Pulsing process; DC sputtering; tin oxide; reactive gas; tuning.

## 1. Introduction

The emergence of multispectral thin-film optoelectronic devices offering high and tuned optical signal powers and photo responses in wide spectrum range (from UV to infrared wavelengths) has opened new pathways for the development of high performance and multifunctional optoelectronic systems [1-5]. Among the variety of optoelectronic devices, broadband photodetectors (PDs) can work in the UV-Vis-IR bands and are of great importance in practical applications including industrial and military fields, such as telecommunications, imaging, spectroscopy, environmental monitoring and missile warning [5-7]. Metal oxide semiconductors such as ZnO, TiO<sub>2</sub>, V<sub>2</sub>O<sub>5</sub>, NiO and CuO are widely used for photodetection applications due to their high stability, earth-abundant property and simple elaboration processes [8-9]. In this regard, several elaboration techniques and materials such as two-dimensional (2D) monolayers, perovskites, nanoparticles and solution-processable materials using spin coating fabrication process have long been investigated aiming at overcoming the main limitations associated with the conventional optoelectronic devices [10-13]. Furthermore, the development of self-powered and tuned multispectral devices using several combined materials and new elaboration approaches has received a great deal of attention to provide high-performance power-free and multispectral optoelectronic devices [12-16]. Nevertheless, various challenges remain to attain the desired stage of maturity of broadband devices for the emerging optoelectronic systems. Particularly, several photodetectors are based on vacuum photomultipliers, which usually feature the advantages of high responsivity under applied bias voltage but suffer from the large operating voltage and high-power dissipation. Moreover, the developed multispectral and self-powered photodetectors based on low cost solution-processable materials exhibit high photoresponse properties, low fabrication cost and flexibility behavior but usually suffer from the presence of toxic elements and stability issues. On the other hand, the unique properties of the

monolayer materials such as the atomic layer thickness and less surface chemical suspension bonds have demonstrated promising effectiveness and led to an extended photosensitivity in different spectral ranges [17, 18]. However, high dark noise as well as the low absorption edge effects of these materials can affect their optoelectronic performances and photosensitivity capabilities. Moreover, similar limitations are associated with other optoelectronic devices based on nanostructure and heterojunction technologies. Therefore, new materials and elaboration techniques are highly required to find suitable approaches to break through these limitations and satisfy the requirements of the next generation of optoelectronic devices.

In recent years, metal oxide materials have been widely investigated and the improvement of their optical and electrical properties is becoming one of extensive research activities [19-21]. Particularly, thin oxide-based alloys ( $\text{SnO}$ ,  $\text{SnO}_2$ ,  $\text{Sn}_2\text{O}_4$ ,...) are regarded as potential candidates for non-toxic and low cost optoelectronic devices [22-24]. In this context, tin dioxides ( $\text{SnO}_2$ ) have been studied to explore its capability to be used in wide application areas, including transparent electrodes (TCO), electrochromic sensors, solar cells and electrocatalysis applications [24]. Moreover, tin monoxide has drawn substantial interests recently as a wide gap p-type oxide with high hole mobility, making it effective for developing thin film transistors (TFTs), organic solar cells (OSCs) and hole transport layers (HTLs) for optoelectronic devices [25-27]. Important optoelectronic properties of tin oxide-based alloys, like carrier concentration, optical band gap, mobility and optical transmission, are drastically varied with increasing the oxygen amount in the tin oxide alloy [25]. Wavelength dependent absorption, optical bandgap parameters, and electrical conductivity of tin oxide alloy are important properties owing to its implementation as buffer, HTL and active layers for optoelectronic applications. Consequently, the impact of oxygen concentration on the tin

oxide alloy properties should be experimentally investigated in order to optimize and tune the optoelectronic performances for photosensing applications.

In this work, we investigate the photoresponse characteristics of a new tunable band selective SnO<sub>x</sub> PD prepared by DC reactive sputtering. The reactive gas pulsing process (RGPP) approach is used to adjust tin and oxygen concentrations in the deposited thin-films. The impact of the pulsed oxygen concentration on the optoelectronic properties are then characterized using XRD, SEM, DC electrical resistivity measurement and UV–Visible absorption spectroscopy techniques to analyze the structure morphological, optical and electrical performances. The deposited thin-films are used to investigate the optoelectronic properties of photodetector with tuned spectral photoresponsivity (UV and broadband multispectral). Here, we also demonstrate that the responsivity and bandwidth can be modulated by adjusting the injection oxygen time in the active layer.

## **2. Experimental details**

### **2.1. Deposition of SnO<sub>x</sub> thin-films**

SnO<sub>x</sub> thin-films were developed on glass and (100) silicon (Si) substrates. The latter were first cleaned up by using the standard RCA sequence process and then dried in an oven at 60 °C. Afterwards, SnO<sub>x</sub> thin-films were deposited on glass substrates (surface area of 1.25×2.5 cm<sup>2</sup> for each one) by using DC reactive magnetron sputtering system in a 40 L vacuum chamber evacuated at 10<sup>-5</sup> Pa of pressure [28]. The DC sputtering system used a constant current density of 50 Am<sup>-2</sup> and a magnetic field level of 600 Gauss was obtained by permanent magnets (FeNdB). The sputtering process was carried out using high purity tin target (99.9 at. %) and the target-to-substrate distance was kept at 65 mm. To sputter deposit SnO<sub>x</sub> thin-films with dissimilar compositions, Ar gas was injected with a partial pressure of 0.3 Pa, while oxygen gas was introduced using the Reactive Gas Pulsing Process (RGPP) to vary the injection time of the oxygen gas [29]. In this context, the oxygen mass flow rate was

pulsed as a function of time based on the pulsing signal depicted in Fig. 1. In the latter figure,  $t_{ON}$  and  $t_{OFF}$  denote the RGPP ON and OFF times of oxygen pulsing associated with the considered rectangular signal,  $P$  is the pulsing period and  $\alpha$  represents the duty cycle defined as  $\alpha = t_{ON}/P$ . During the sputtering process,  $P$  was kept at 20 s, whereas  $\alpha$  varied from 0 to 100% of  $P$ , enabling a gradual variation of  $\alpha$ , where the maximum and minimum oxygen flow rates were fixed at 2.4 sccm and 0 sccm over  $t_{ON}$  and  $t_{OFF}$  times, respectively. SnO<sub>x</sub> thin-film samples using different  $t_{ON}$  values of 0 s, 8 s, 10 s, 12 s, 16 s and 20 s were produced to assess the effect of the RGP process on the film properties. For some given  $t_{ON}$  and  $t_{OFF}$  values, the operating conditions allow reaching the oxidized sputtering mode during  $t_{ON}$ , while completely stopping the oxidation process during  $t_{OFF}$ . The deposition time was adjusted for all samples to obtain a specific SnO<sub>x</sub> film thickness of 400 nm, which was confirmed using a profilometer Alpha-step IQ, KLA-Tencor Corporation. Finally, E-Beam evaporation technique was used to fabricate SnO<sub>x</sub>-based Metal-Semiconductor-Metal (MSM) photodetectors. In this context, gold (Au) contacts were evaporated on the SnO<sub>x</sub> films sputter-deposited at various pulsing times by means of a shadow mask with a rectangular surface of 2.5 mm<sup>2</sup> and electrode distance of  $L = 7$  mm.

## 2.2. Characterization

X-ray diffraction (XRD) measurements using ARL Equinox 300 diffractometer were performed to study the structural properties of the elaborated SnO<sub>x</sub> thin-films based on the reactive gas pulsing process. Besides, scanning electron microscope (SEM) characterizations were carried out to view the top surface of the prepared SnO<sub>x</sub> thin-films on Si substrate at various pulsing times ranging from  $t_{ON} = 8$  s to  $t_{ON} = 20$  s using JEOL JSM 7800 field emission SEM apparatus. The elaborated samples on Silicon substrates were used only to carry out high quality cross-sectional SEM images and to better study the morphological properties of SnO<sub>x</sub> thin-films elaborated using RGPP. Besides, the energy dispersive X-ray

spectroscopy (EDS) measurements were carried out using EDAX system (FEI Quanta 450), to determine oxygen and tin elemental concentrations in the deposited SnO<sub>x</sub> thin-films using RGPP. In addition, F10-RT-UV-based spectrophotometer was exploited to extract the wavelength dependent optical parameters including absorbance and reflectance of the prepared SnO<sub>x</sub> samples. Hall measurements were conducted to assess the electrical properties of the sputter-deposited SnO<sub>x</sub> thin-films with various pulsing times and the associated film resistivity values were extracted. Afterwards, the semiconductor characterization system (Keithley 4200-SCS) was then used to extract the current-voltage (I-V) characteristics of the prepared MSM PD samples based on sputtered SnO<sub>x</sub> active layer at different oxygen pulsing times. The associated I-V curves were extracted under dark and UV-Vis-NIR illumination conditions for all samples. The photoresponse characteristics of the prepared band-selective PDs based on SnO<sub>x</sub> thin-films were analyzed using UV, Visible and NIR LED lamps. The emission wavelengths of the UV, Visible, and NIR LEDs were 365 nm, 515 nm–525 nm, and 780 nm–950 nm, respectively. The output optical power densities of these LEDs were measured as 1.8, 2.3, and 3.7 mW/cm<sup>2</sup>. All measurements were carried out in room temperature conditions.

### **3. Results and discussions**

To assess the structural properties of the elaborated SnO<sub>x</sub> thin-films at various pulsing times, XRD measurements were carried out and the corresponding patterns are depicted in Fig. 2. The latter figure confirms that the prepared sample at  $t_{ON} = 0$  s shows diffraction peaks associated with tetragonal Sn material (ICDD card no. 00-004-673). The use of RGPP allows sputter-depositing SnO<sub>x</sub> thin-films with tunable compositions, leading to metallic form at  $t_{ON} = 0$  s [30]. On the other hand, low intensity peaks from (200), (101), (220) and (211) planes are observed for the elaborated sample with oxygen pulsing time of  $t_{ON} = 4$  s. When the oxygen gas is pulsed with 8 s, 12 s, 16 s and 20 s of ON-time, the elaborated SnO<sub>x</sub> thin-films

exhibit amorphous states as it is shown in the associated XRD patterns, where no diffraction peaks are observed. This is mainly attributed to the effect of oxygen containing, disturbing the growth of crystalline phases in the developed SnO<sub>x</sub> thin-films. In addition, the periodic injection of the reactive gas using RGPP prevents the formation of metal oxide compound on the target surface [30-31]. Intuitively, the use of an appropriate thermal treatment can enhance the film crystallinity.

Fig.3 (a) shows the variation of the deposition rate as a function of the oxygen pulsing time. It can be seen from this figure that the deposition rate gradually decreases as the oxygen pulsing time rises. This reduction can be correlated with the poisoning of the tin target surface by the oxygen, giving rise to a reduced sputtering yield compared to that of Sn. The variation of tin and oxygen concentrations in the prepared SnO<sub>x</sub> thin-films as a function of the oxygen pulsing time is measured and depicted in Fig. 3 (b). It can be seen that the elemental composition in the film continuously varies with the variation of the oxygen pulsing time ( $t_{ON}$ ). As  $t_{ON}$  increases, the oxygen content increases in the film, while the tin concentration symmetrically decreases. This typically observed in oxide thin films prepared by RGPP since an alternation of the sputtering mode from metallic to oxidation one occurs. In other words, the oxygen flow rate rapidly increases to achieve its maximum (2.4 sccm) during the  $t_{ON}$  time, leading to avalanche the deposition procedure in the oxidation mode. On the other hand, the oxygen mass flow rate is completely stopped during the  $t_{OFF}$  time, thus switching the sputtering process to the metallic mode. Fig.3 (b) demonstrates also that the chemical composition of SnO<sub>x</sub> thin-films can be tuned by adjusting the oxygen pulsing time, where high oxygen content compounds can be elaborated by taking large  $t_{ON}$  values. It can be also observed from Fig.3 (b) that the most important variation of SnO<sub>x</sub> composition is achieved for  $t_{ON}$  values lower than 16 s, where the sputtered thin-films gradually evolve from sub- to over-stoichiometric SnO<sub>x</sub> compounds.

SEM measurements were performed to investigate the morphological properties of the prepared SnO<sub>x</sub> thin-films using RGPP with different pulsing times. Fig. 4 illustrates the obtained micrographs with high magnification of the sputtered SnO<sub>x</sub> samples with (a)  $t_{ON} = 0$  s, (b)  $t_{ON} = 8$  s, (c)  $t_{ON} = 12$  s and (d)  $t_{ON} = 20$  s. It can be observed from Fig. 4 (a) that the sputtered film with  $t_{ON} = 0$  s shows continuous and granulated surface properties with small gaps between grains. In this situation, the oxygen mass flow rate is stopped, and the sputtering process is switched to the metallic mode. As a result, Sn thin-film is produced with irregularly shaped grain morphology. This leads to sputter a large number of Sn particles on the substrate, which have high mobility thereby allowing the formation of large clusters. This observation agrees well with the obtained XRD patterns presented in Fig. 2, where sharp peaks associated with Sn material are observed. As the pulsing time increases, it can be seen from Fig. 4 (b) that the grains become sphere-like shapes with lower grain size. Besides, a smooth surface is observed when the oxygen flow rate is increased. Further increasing the ON-time results in smooth and dense accumulation film as it is observed in Fig. 4 (c) and (d) under similar SEM magnification. The increase of the duty cycle ( $\alpha > 80$  % of P) favors the oxidation sputtering mode [31]. This can in turn drop the deposition rate and maintain the oxygen concentration stable as it is shown in Fig.3 (a) and (b). The latter figure demonstrates that the growth of SnO<sub>x</sub> thin-films using high duty cycle ( $\alpha > 80$  % of P) leads to achieve oxygen-rich films, indicating that the oxidation sputtering mode is the dominant one under these deposition conditions. Consequently, the sputtered Sn particles are rapidly oxidized, enabling the formation of Sn–O bonds and thereby typical amorphous SnO<sub>x</sub> thin-films are produced as it is confirmed by measured XRD patterns. Cross-sectional SEM images of the deposited SnO<sub>x</sub> thin-films using different oxygen pulsing times of 0 s, 12 s and 20 s are shown in Fig.4 (e), (f) and (g), respectively. Various morphologies as a function of the oxygen pulsing time are observed. In the metallic sputtering mode ( $t_{ON} = 0$  s), Fig.4 (e) shows a

microstructured films with a more or less obvious columnar structure. On the other hand, Fig.4 (f) and (g) indicate that homogeneous and denser SnO<sub>x</sub> thin-films are elaborated by increasing the oxygen pulsing time. Despite the fact that RGPP gives multilayered structure (metal/oxide periodic alternations) [30-33], the use of a short pulsing period (P=20 s) and a quite low deposition rate (about 1000 nmh<sup>-1</sup>) allows preparing homogeneous tin oxide thin-films rather than multilayer structure [33].

In order to analyze the performance of the developed SnO<sub>x</sub> thin-films for photodetection applications, the optical absorbance and reflectance spectra in the visible range of the samples prepared on glass substrates with dissimilar duty cycles are extracted and depicted in Fig. 5 (a) and (b), respectively. We can notice that the fabricated film at  $t_{ON} = 0$  s fully absorbs the incident light due to its metallic behavior. Increasing the duty cycle leads to gradually decrease the absorption capabilities of the SnO<sub>x</sub> thin-film. Particularly, the developed films with high  $t_{ON}$  time of 16 s and 20 s show a high UV absorbance with solar-blind characteristic. This is mainly due to the high oxygen concentration associated with these SnO<sub>x</sub> thin-films when continuous oxidation process is considered, leading to enhance the visible transparency. On the other hand, a transition zone is observed between the lowest and highest duty cycles, where the associated films ( $t_{ON} = 10$  s and  $t_{ON} = 12$  s) can offer larger absorption band extended to blue and red lights as compared to the prepared SnO<sub>x</sub> thin-films with high  $t_{ON}$  duration. This optical behavior is attributed to the evolution of Sn and O contents as a function of the  $t_{ON}$  increment, leading to change the sputtered thin-films from sub- to over-stoichiometric SnO<sub>x</sub> compounds as it is shown in Fig.3 (b). The reflectance spectra depicted in Fig.5 (b) show the presence of typical interference fringes over the visible region, indicating that the associated SnO<sub>x</sub> thin-films are homogenous and their surface is smooth. This is ascribed to the high oxygen concentration of these films. The optical band gap of the prepared SnO<sub>x</sub>-based samples with dissimilar pulsing times is estimated from the

associated Tauc's plots shown in Fig. 5 (c), assuming direct transitions. It is clearly shown from this figure that the  $\text{SnO}_x$  thin-film band gap increases as the duty cycle increases to reach the highest value of  $E_{g4} = 3.58$  eV corresponding to over-stoichiometric  $\text{SnO}_2$  compound [34]. However, a lower band gap value of  $E_{g1} = 1.8$  eV is achieved for the elaborated  $\text{SnO}_x$  thin-film with short pulsing time of 8 s. This phenomenon can be attributed to the role of using RGPP in adjusting the Sn and O concentrations in the sputtered  $\text{SnO}_x$  thin-films. Therefore, the obtained optical behavior indicates that multispectral PDs and solar-blind UV PDs can be realized by well controlling the RGPP during the sputter deposition of  $\text{SnO}_x$  thin-films.

Aiming at investigating the photoresponse properties of the fabricated  $\text{SnO}_x$  thin-films with various oxygen pulsing times, top electrodes were realized on the prepared  $\text{SnO}_x/\text{Glass}$  samples to form an MSM configuration. The associated I-V characteristics under dark and UV-illumination conditions are extracted and illustrated in Fig. 6 (a) and (b), respectively. It can be noticed from Fig. 6 (a) that the prepared  $\text{SnO}_x$ -PD with the highest duty cycle of 100% of P ( $t_{\text{ON}} = 20$  s) corresponding to continuous oxidation process exhibits the lowest dark current of 3.7 nA as compared to other samples (0.44  $\mu\text{A}$  and 0.16  $\mu\text{A}$ ) with lower oxygen pulsing times of 10 s and 12 s, respectively. This is mainly due to its high resistivity of  $1.9 \times 10^4 \Omega\text{m}$  as compared to the other devices (4.82  $\Omega\text{m}$  and 187  $\Omega\text{m}$ ). This high resistivity value can be attributed to the formation of O-rich  $\text{SnO}_x$  compound when high duty cycle is considered. Under UV light exposure, the prepared  $\text{SnO}_x$ -based PDs show a high photoresponse characteristics, where high photocurrents in the order of few microamperes is achieved for the elaborated samples using dissimilar oxygen pulsing times. Moreover, the elaborated device produced with a low pulsing time shows the highest photocurrent value of 9  $\mu\text{A}$ . This can be explained by the low resistivity and the high absorbance of the corresponding  $\text{SnO}_x$  film, promoting enhanced photogeneration of e/h pairs and improved carrier extraction capability. In addition, the prepared device using the highest pulsing time (20 s) exhibits the

best ON-to-OFF current ratio due to its very low dark current. The prepared devices using oxygen pulsing times of 8 s, 12 s and 20 s, show high signal-to-noise (SN) ratio values of  $2.2 \times 10^3$ ,  $3.1 \times 10^3$  and  $6 \times 10^4$ , respectively. This indicates the low noise effects of the prepared SnO<sub>x</sub>-based PDs. The obtained photoresponse characteristic can be explained by the high absorption capability over the UV spectral band of the prepared SnO<sub>x</sub> thin-films. To further evaluate the elaborated SnO<sub>x</sub>-based PDs for multispectral photodetection property, the responsivity spectra of the prepared samples using various pulsing times are measured and shown in Fig. 7. It can be seen from this figure that the fabricated device based on SnO<sub>x</sub> thin-film with  $t_{ON} = 20$  s demonstrates a high responsivity of 22.3 mA/W over the UV range ( $R_{UV}$ ) at an applied voltage of 3 V and an optical power of 1.8 mW/cm<sup>2</sup>. In addition, a high rejection ratio ( $R_{ratio} = R_{UV}/R_{vis}$ ) of  $R_{ratio} = 1.1 \times 10^4$  is achieved, thus emphasizing its solar-blind characteristic. Interestingly, the prepared SnO<sub>x</sub>-PD with  $t_{ON} = 12$  s promotes extended photoresponse characteristics to blue light, offering high responsivity values of  $R_{UV} = 28$  mA/W and  $R_{vis} = 16$  mA/W over the UV and visible spectral bands, respectively. In addition, the device based on the fabricated SnO<sub>x</sub> thin-film with 8 s of pulsing time demonstrates broadband photodetection capabilities with a high photoresponse exceeding 30 mA/W. This behavior correlates well with the obtained band gap and optical absorption variation as the oxygen pulsing time is changed during the sputtering process. Therefore, this photoresponse analysis is expected to give extensive details to the designer for getting expert knowledge concerning the spectral sensing ability of the analyzed PDs based on the elaborated SnO<sub>x</sub> thin-films with various oxygen pulsing times. Accordingly, the use of high duty cycle offers the possibility for designing high-performance low-noise solar-blind UV PDs, while the implementation of RGPP during the sputtering process of SnO<sub>x</sub> thin-films with controlled pulsing times opens up new pathways to develop cost-effective multispectral UV-Vis PDs.

Table.1 recapitulates a performance comparison between the elaborated SnO<sub>x</sub> PDs and others devices reported on recently published works for different excitation spectral bands [33-40]. The latter are selected focusing on SnO<sub>x</sub>-based PDs and cost-effective CRM-free metal oxide-based structures to perform a systematic comparison. It can be demonstrated from results reported in Table 1 that the PD based on the prepared SnO<sub>x</sub> thin-film with high duty cycle provides enhanced UV responsivity ( $R = 21.8 \text{ mA/W}$  at an applied voltage of 3 V and an optical power of  $1.8 \text{ mW/cm}^2$ ), detectivity ( $D^* = 5.8 \times 10^{11} \text{ Jones}$ ) and ON-to-OFF ratio ( $I_{\text{ON}}/I_{\text{OFF}}$  ratio = 55.3 dB) as compared to other designs. This confirms its capability for solar blind UV photodetection applications. It can be also concluded from Table.1 that the investigated PD based on sputtered SnO<sub>x</sub> thin-film using  $t_{\text{ON}} = 12 \text{ s}$  offers extended photoresponse characteristics, showing a high responsivity ( $R = 19 \text{ mA/W}$  at an applied voltage of 3 V and an optical power of  $2.3 \text{ mW/cm}^2$ ) and detectivity ( $D^* = 1.1 \times 10^{11} \text{ Jones}$ ) over the visible spectral band. This proves its capability for multispectral sensing applications. More importantly, further extension of the photosensing band is achieved by introducing RGPP with  $t_{\text{ON}} = 8 \text{ s}$ , where broadband responsivity with high value exceeding  $R = 36 \text{ mA/W}$  at an applied voltage of 3 V is recorded. However, the latter SnO<sub>x</sub>-based PD shows degraded detectivity ( $D^* = 9.5 \times 10^{10} \text{ Jones}$ ) and current ratio ( $I_{\text{ON}}/I_{\text{OFF}}$  ratio = 26 dB) as compared to the prepared device using the highest duty cycle ( $I_{\text{ON}}/I_{\text{OFF}}$  ratio = 55.3 dB). This is mainly due to the high dark current, which can be explained by the high conductivity of the sputtered SnO<sub>x</sub> thin-film owing to the high Sn content when the shortest duty cycle is considered. Therefore, the obtained photodetection characteristic is a clear indication of the crucial role of using controlled RGPP for the elaboration of tunable band-selective PDs based on cost-effective SnO<sub>x</sub> thin-film, a feature that is distinctively regarded superior to traditional devices.

Further improvements regarding the PD performance can be achieved by investigating the effect of interfacial defects, temperature and surface morphology on the device

photoresponse characteristics. In addition, further measurements regarding the ageing and reliability effects should be carried out using appropriate experimental facilities to assess the device stability and reproducibility. This step is considered as a perspective of the present work, new characterizations should be performed.

#### **4. Conclusion**

In this paper, a new high-performance tunable band-selective PD based on DC sputtered SnO<sub>x</sub> thin-films using controlled reactive gas pulsing process (RGPP) is demonstrated. The RGPP is used to tune the Sn and oxygen containing in the SnO<sub>x</sub> thin-films, where a rectangular pulsing signal with various pulsed oxygen times ranging from 0 s to 20 s is considered. The structural, surface morphology and optical properties of the prepared samples are investigated by carrying out effective XRD, SEM and spectroscopy characterizations. It is revealed that the prepared SnO<sub>x</sub> thin-films show an amorphous state and tunable optical and electronic properties, where by varying the pulsed oxygen time in the range of [8 s, 20 s] the absorbance behavior is modulated and the optical band gap is changed from 1.9 eV to 3.56 eV. More importantly, it was revealed that the SnO<sub>x</sub> PD sensing band depends on the ON pulsing time associated with RGPP. In this context, solar-blind low-noise UV PD can be tuned by considering the highest ON pulsing time during the sputtering process of SnO<sub>x</sub> sensing film, while the use of low duty cycles opens up new pathway for the fabrication of multispectral PDs. Therefore, the present investigation can provide new guidelines for the realization of tunable band-selective PDs based on sputtered SnO<sub>x</sub> thin-films, which is suitable for the emerging multifunctional optoelectronic devices.

## References

- [1] L. Colace, V. Soriano, S. Rajamani, “Investigation of Static and Dynamic Characteristics of Optically Controlled Field Effect Transistors”, *J. Light. Technol.* vol. 32, pp. 2233-2239, 2014.
- [2] N. Ding, et al., “A novel approach for designing efficient broadband photodetectors expanding from deep ultraviolet to near infrared”, *Light: Science & applications*, vol.91, pp. 1-13, 2022.
- [3] J. Michel, J. Liu, L. C. Kimerling, “High-performance Ge-on-Si photodetectors”, *Nat. Photonics*, vol. 4, no. 8, pp. 527–534, 2010.
- [4] A. Shyam, N. Kumar, A. Kaitheri, R. Raju and R. Swaminathan, “Self-Powered UV Photodetectors Based on Heterojunctions Composed of ZnO Nanorods Coated with Thin Films of ZnS and CuI,” *ACS Appl. Nano Mater.*, vol. 10, pp. 8529–8539, 2023.
- [5] X. Liu, et al., “Transparent, High-Performance Thin-Film Transistors with an InGaZnO/Aligned-SnO<sub>2</sub>-Nanowire Composite and their Application in Photodetectors”, *Adv. Mater.*, vol. 26, pp. 7399-7404, 2014.
- [6] R. Balakarthikeyan, A. Santhanam, R. Anandhi, S. Vinoth, A. M. Al-Baradi, Z. A. Alrowaili, M. S. Al-Buriah, K. D. A. Kuma, “Fabrication of nanostructured NiO and NiO:Cu thin films for high-performance ultraviolet photodetector”, *Opt. Mater.*, vol. 120, pp. 111387-11, 2021.
- [7] H. Yu, X. Liu, L. Yan, T. Zou, H. Yang, C. Liu, S. Zhang, H. Zhou, “Enhanced UV-visible detection of InGaZnO phototransistors via CsPbBr<sub>3</sub> quantum dots”, *Semicond. Sci. Technol.* vol. 34, pp. 25013-8, 2019.
- [8] A. Pimentel, S. H. Ferreira, D. Nunes, T. Calmeiro, R. Martins and E. Fortunato, “Microwave Synthesized ZnO Nanorod Arrays for UV Sensors: A Seed Layer Annealing Temperature Study”, *Materials*. vol. 9, pp. 299-15, 2016.
- [9] D. Nunes, A. Pimentel, A. Gonçalves, S. Pereira, R. Branquinho, P. Barquinha, E. Fortunato and R. Martins, “Metal oxide nanostructures for sensor applications”, *Semicond. Sci. Technol.* vol. 34, pp. 043001, 2019.
- [10] Y. Zhai, G. Chen, J. Ji, Z. Wu, Y. Li, Q. Wang, “Investigation of photocurrent transient variation in Au nanoparticles decorated IGZO phototransistor”, *Phys. E: Low-Dimens. Syst. Nanostructures*, vol. 113, pp. 92–96, 2019.
- [11] P. Zhang, Y. Zhang, W. Wang, L. Gao, G. Li, S. Zhang, J. Lu, Y. Yu and J. Zhang, “Multispectral photodetectors based on 2D material/Cs<sub>3</sub>Bi<sub>2</sub>I<sub>9</sub> heterostructures with high detectivity”, *Nanotechnology*, vol. 32, pp. 415202, 2021.

- [12] D. J. Norris, “Multispectral quantum-dot photodetectors”, *Nature Photonics*, vol. 13, pp. 230–232, 2019.
- [13] Z. Zhao, C. Xu, L. Niu, X. Zhang, F. Zhang, “Recent Progress on Broadband Organic Photodetectors and their Applications”, *Laser Photonics Rev.*, vol. 14 pp. 2000262-24, 2020.
- [14] R. Pant, D. K. Singh, A. M. Chowdhury, B. Roul, K. K. Nanda, S. B. Krupanidhi, “Next-generation self-powered and ultrafast photodetectors based on III-nitride hybrid structures”, *APL Mater.*, vol. 8, pp. 020907-11, 2020.
- [15] A. M. Chowdhury, G. Chandan, R. Pant, B. Roul, D. K. Singh, K. K. Nanda, S. B. Krupanidhi, “Self-Powered, Broad Band, and Ultrafast InGaN-Based Photodetector”, *ACS Appl. Mater. Interfaces*, vol. 11, pp. 10418–10425, 2019.
- [16] K. L. Kumawat, D. K. Singh, K. K. Nanda, S. B. Krupanidhi, “Solution-Processed SnSe<sub>2</sub>-RGO-Based Bulk Heterojunction for Self-Powered and Broadband Photodetection”, *ACS Appl. Electron. Mater.*, vol. 3, pp. 3131-3138, 2021.
- [17] S. Maity, K. Sarkar, P. Kumar, “A progressive journey into 2D-chalcogenide/carbide/nitride-based broadband photodetectors: recent developments and future perspectives”, *J. Mater. Chem. C*, vol. 9, pp. 14532-14572, 2021.
- [18] J. R. K. Ulaganathan, R. Sankar, C-Y. Lin, R. C. Murugesan, K. Tang, F-C. Chou, “High-Performance Flexible Broadband Photodetectors Based on 2D Hafnium Selenosulfide Nanosheets”, *Adv. Electron. Mater.*, vol. 6, pp. 1900794-9, 2020.
- [19] H. Ferhati, F. Djeflal, N. Martin, “Highly improved responsivity of self-powered UV–Visible photodetector based on TiO<sub>2</sub>/Ag/TiO<sub>2</sub> multilayer deposited by GLAD technique: Effects of oriented columns and nano-sculptured surface”, *App. Surf. Sci.*, vol. 529, pp. 147069-10, 2020.
- [20] C. L. Hsu, H. Y. Wu, C. C. Fang, S. P. Chang, “Solution-Processed UV and Visible Photodetectors Based on Y-Doped ZnO Nanowires with TiO<sub>2</sub> Nanosheets and Au Nanoparticles”, *ACS Appl. Mater. Interfaces*, vol.5, pp. 2087-2095, 2018.
- [21] G. Chatzigiannakis, A. Jaros, R. Leturcq, J. Jungclaus, T. Voss, S. Gardelis, M. Kandyla, “Laser-Microstructured ZnO/p-Si Photodetector with Enhanced and Broadband Responsivity across the Ultraviolet–Visible–Near-Infrared Range”, *ACS Appl. Electron. Mater.*, vol.9, pp. 2819–2828, 2020.
- [22] A. K. Singh, A. Janotti, M. Scheffler, C.G. Van de Walle, “Sources of electrical conductivity in SnO<sub>2</sub>”, *Phys. Rev. Lett.*, vol. 101, pp. 055502-4, 2008.

- [23] D. O. Scanlon, “Defect engineering of BaSnO<sub>3</sub> for high-performance transparent conducting oxide applications”, *Phys. Rev. B*, vol. 87, pp. 161201-5, 2013.
- [24] G. K. Dalapati et al., “Tin oxide for optoelectronic, photovoltaic and energy storage devices: a review”, *J. Mater. Chem. A*, vol. 9, pp. 16621–16684, 2021.
- [25] C. K. G. Kwo, Y. Wang, X. Shu and K. M. Yu, “Conversion of p-type SnO to n-type SnO<sub>2</sub> via oxidation and the band offset and rectification of an all-Tin oxide p-n junction structure”, *Appl. Surf. Sci.*, vol. 627, pp. 157295-7, 2023.
- [26] R. Barros, K. J. Saji, J. C. Waerenborgh, P. Barquinha, L. Pereira, E. Carlos, R. Martins, and E. Fortunato, “Role of Structure and Composition on the Performances of P-Type Tin Oxide Thin-Film Transistors Processed at Low-Temperatures”, *Nanomaterials*, vol. 627, pp. 320-18, 2019.
- [27] K. Nomura, “Ambipolar Oxide Thin-Film Transistor”, *Adv. Mater.*, vol. 23, pp. 3431-3434, 2011.
- [28] N. Martin, J. Lintymer, J. Gavaille, J. M. Chappe, F. Sthal, J. Takadoum, F. Vaz, L. Rebouta, “Reactive sputtering of TiO<sub>x</sub>Ny coatings by the reactive gas pulsing process. Part I: pattern and period of pulses”, *Surf. Coat. Technol.* Vol. 201, pp. 7720-7726, 2007.
- [29] E. Aubry, S. Weber, A. Billard, N. Martin, “Enhanced tunability of the composition in silicon oxynitride thin films by the reactive gas pulsing process”, *Appl. Surf. Sci.*, vol. 290, pp. 148-153, 2014.
- [30] A. Cacucci, V. Potin, L. Imhoff, N. Martin, “Structural and electrical properties in tungsten/tungsten oxide multilayers”, *Thin Solid Films*, vol. 553, pp. 93-97, 2014.
- [31] N. Parreira, T. Polcar, A. Cavaleiro, “Characterization of W-O coatings deposited by magnetron sputtering with reactive gas pulsing”, *Surf. Coat. Technol.*, vol.201, pp. 5481-5486, 2007.
- [32] M. Grafouté, C. Petitjean, A. Diama, J. F. Pierson, J. M. Greneche, C. Rousselot, “Structural investigations of iron oxynitride multilayered films obtained by reactive gas pulsing process,” *Surf. Coat. Technol.*, vol. 272, pp. 158-164, 2015.
- [33] X. Xu, M. A. P. Yazdi, R. Salut, J-M. Cote, A. Billard, N. Martin, “Structure, composition and electronic transport properties of tungsten oxide thin film sputter-deposited by the reactive gas pulsing process,” *Mater. Chem. Phys.*, vol. 205, pp. 391-400, 2018.
- [34] M. Kam, Q. Zhang, D. Zhang and Z. Fan, “Room-temperature sputtered SnO<sub>2</sub> as Robust electron transport Layer for Air-Stable and Efficient perovskite solar Cells on Rigid and Flexible substrates”, *Sci. Rep.*, vol. 9, pp. 6963-11, 2019.

- [35] Z. Zhang, Y. Ning, X. Fang, "From nanofibers to ordered ZnO/NiO heterojunction arrays for self-powered and transparent UV photodetectors", *J. Mater. Chem. C*, vol. 7, pp. 223-229, 2019.
- [36] Y. Zhang, W. Xu, X. Xu, J. Cai, W. Yang, X. Fang, "Self-Powered Dual-Color UV–Green Photodetectors Based on SnO<sub>2</sub> Millimeter Wire and Microwires/CsPbBr<sub>3</sub> Particle Heterojunctions", *J. Phys. Chem. Lett.*, vol. 10, pp. 836–841, 2019.
- [37] J. Xue, et al., "UV-blue photodetectors based on n-SnOx/p-diamond heterojunctions", *Mater. Lett.*, vol. 257, pp. 126621-4, 2019.
- [38] M. Athira, S. P. Bharath, S. Angappane, "SnO<sub>2</sub>-NiO heterojunction based self-powered UV photodetectors", *Sens. Actuator. A. Phys.*, vol. 257, pp. 113540-9, 2022.
- [39] J. P. B. Silva, et al., "High-performance self-powered photodetectors achieved through the pyro-phototronic effect in Si/SnOx/ZnO heterojunctions", *Nano Energy*, vol. 89, pp. 106347-10, 2021.
- [40] Y. Zhang, M. Hu, Z. Wang, "Enhanced performances of p-si/n-ZnO self-powered photodetector by interface state modification and pyro-phototronic effect", *Nano Energy*, vol. 71, pp. 104630-9, 2020.
- [41] H. Ferhati, F. Djeflal, "High-Responsivity MSM Solar-Blind UV Photodetector Based on Annealed ITO/Ag/ITO Structure Using RF Sputtering", *IEEE Sens. J.*, vol. 19, pp. 7942-7949, 2019.
- [42] Z. Zheng, L. Gan, J. Zhang, F. Zhuge, T. Zhai, "An enhanced UV–Vis–NIR and flexible photodetector based on electrospun ZnO nanowire array/PbS quantum dots film heterostructure", *Adv. Sci.*, vol.4, pp.1600316-9, 2017.

**Figures caption:**

**Figure.1:** Schematic representation of oxygen mass flow rate as function of time used for RGPP depositions of tin oxide films.

**Figure.2:** X-ray diffraction patterns of the deposited tin oxide films with various oxygen pulsing times, ranging from 0 s to 20 s.

**Figure.3:** (a) Variation of the deposition rate as a function of the oxygen pulsing time. (b) Oxygen and tin atomic concentrations in the sputtered SnO<sub>x</sub> thin-films as a function of the oxygen pulsing time.

**Figure.4:** SEM images of tin oxide thin films deposited on silicon substrate with various oxygen pulsing times: (a)  $t_{ON} = 0$  s, (b)  $t_{ON} = 8$  s, (c)  $t_{ON} = 12$  s, (d)  $t_{ON} = 20$  s. (e), (f) and (g) Cross-sectional SEM micrographs of SnO<sub>x</sub> thin-films deposited using oxygen pulsing times of  $t_{ON} = 0$  s,  $t_{ON} = 12$  s and  $t_{ON} = 20$  s, respectively.

**Figure.5:** (a) Absorbance and (b) reflectance spectra (c) Tauc plots in the visible range of the prepared SnO<sub>x</sub> structures using various oxygen pulsing times ranging from 0 s to 20 s.

**Figure.6:** I-V characteristics of the elaborated PD devices based on sputtered SnO<sub>x</sub> thin-films using RGPP with various oxygen pulsing times: (a) dark currents (b) under UV illumination.

**Figure.7:** Responsively variations for different oxygen pulsing times:  $t_{ON} = 8$  s, (b)  $t_{ON} = 12$  s,  $t_{ON} = 20$  s.

**Tables:**

**Table.1:** Performance comparison between the prepared PDs based on SnO<sub>x</sub> thin-films prepared with different pulsing times and several recently published works on UV and multispectral PD devices.

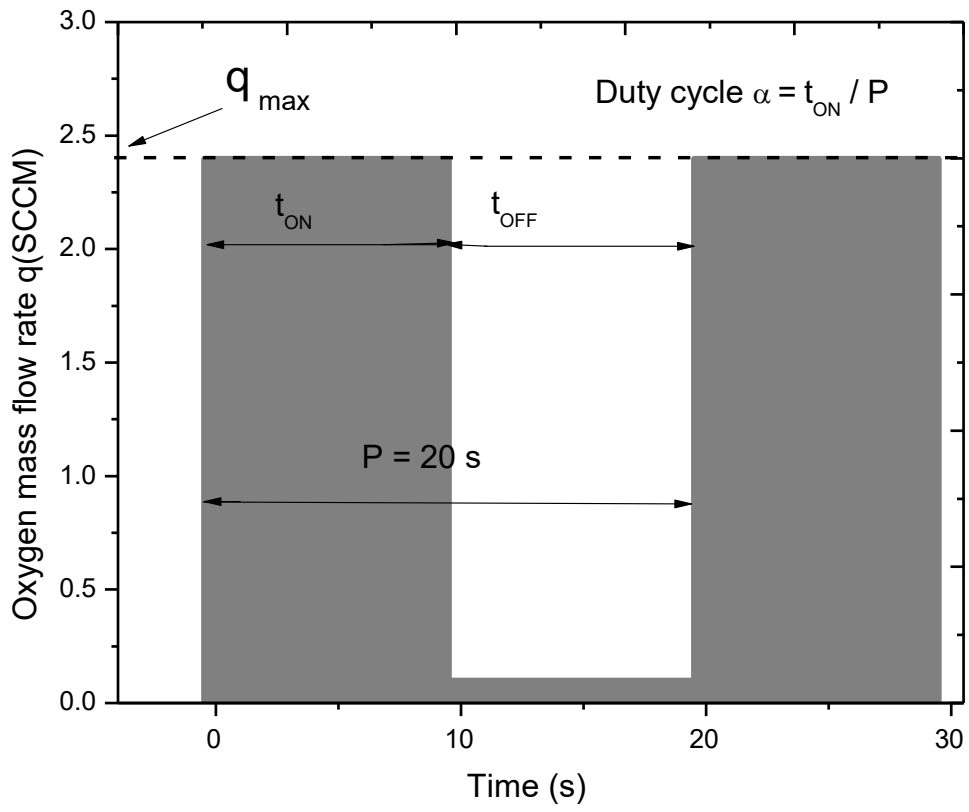


**Figure.1**

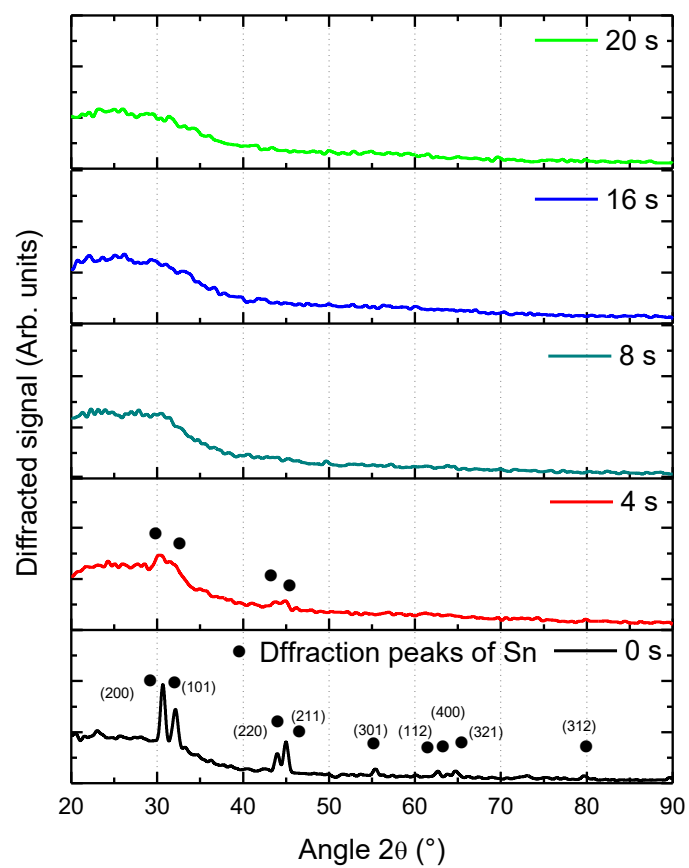
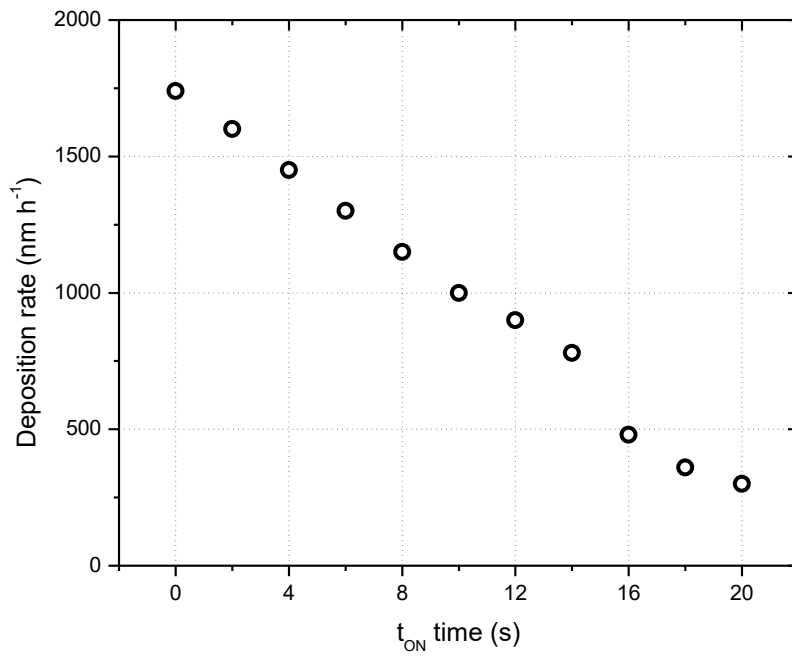
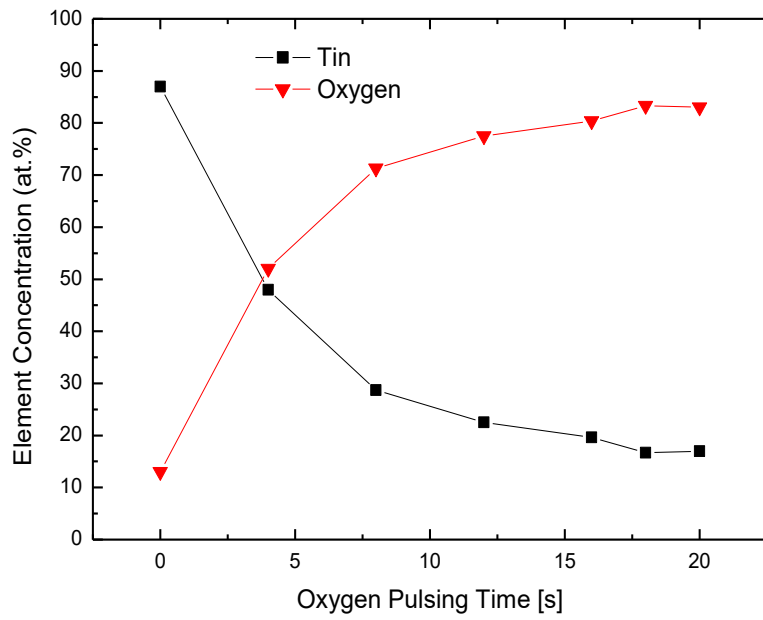


**Figure.2**



(a)



(b)

Figure.3

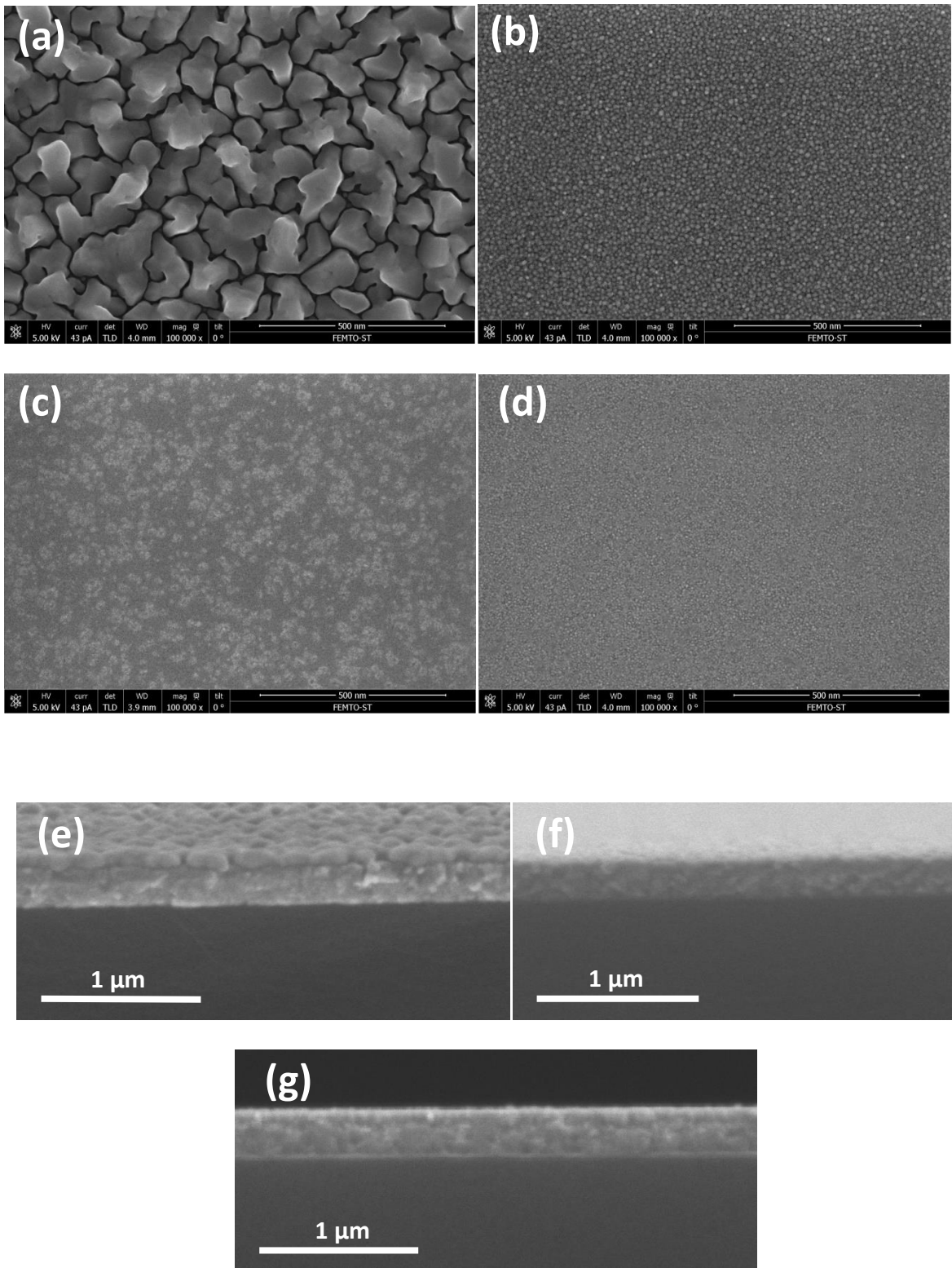
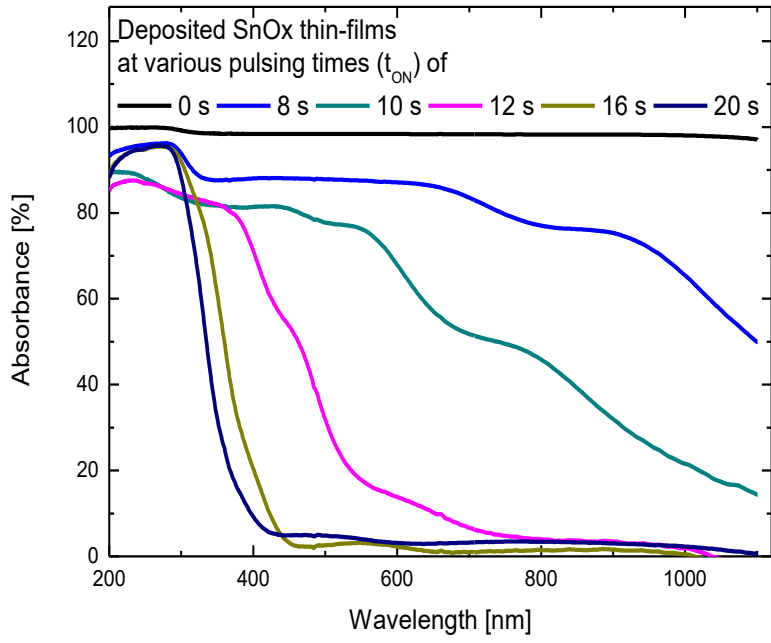
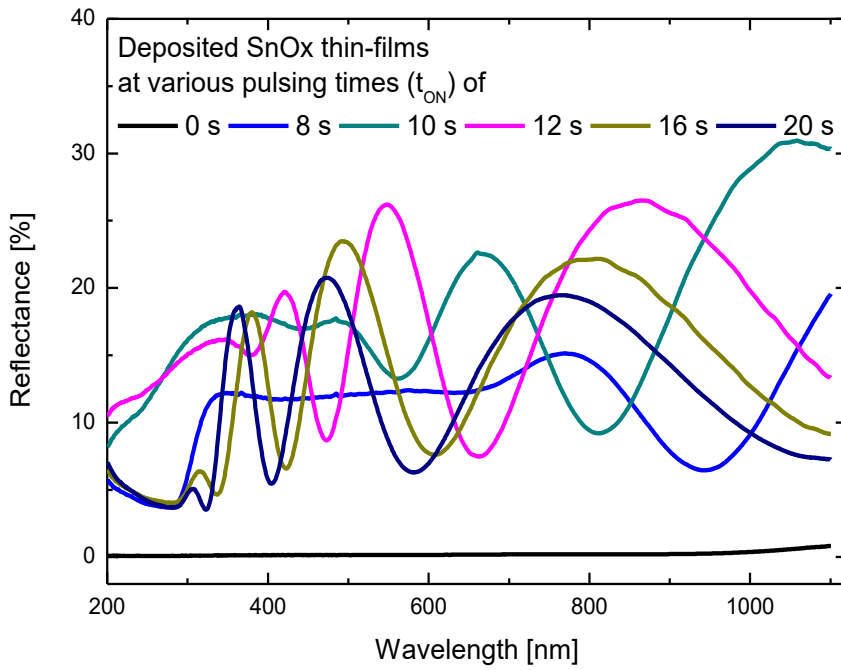


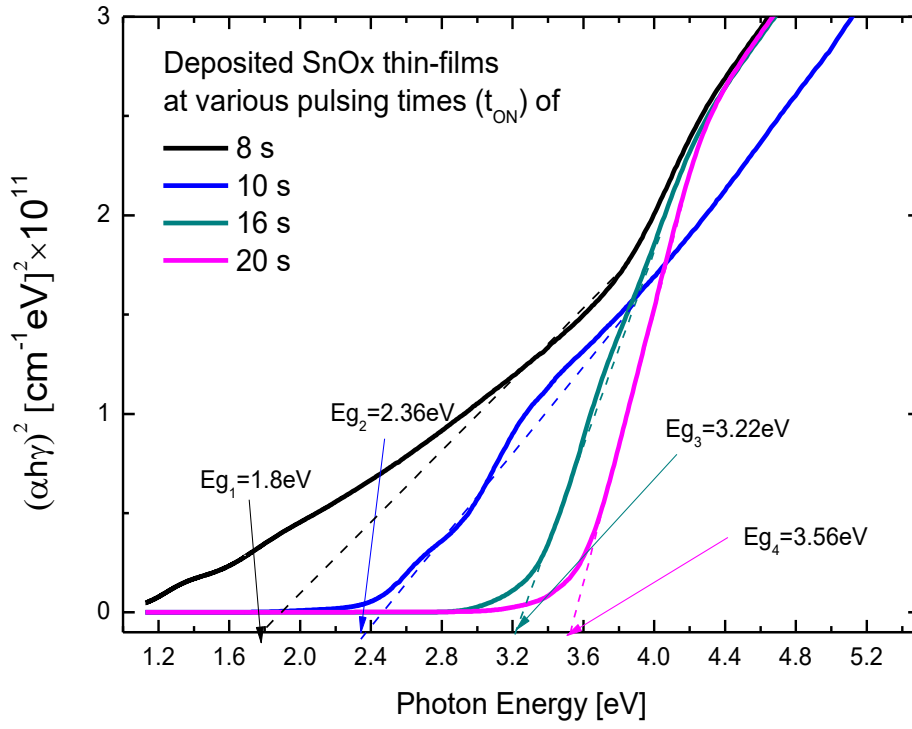
**Figure.4**



(a)

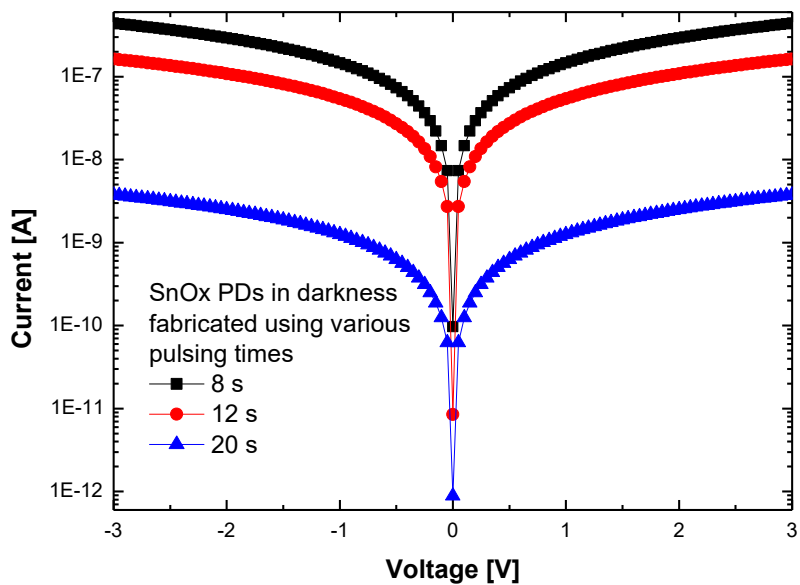


(b)

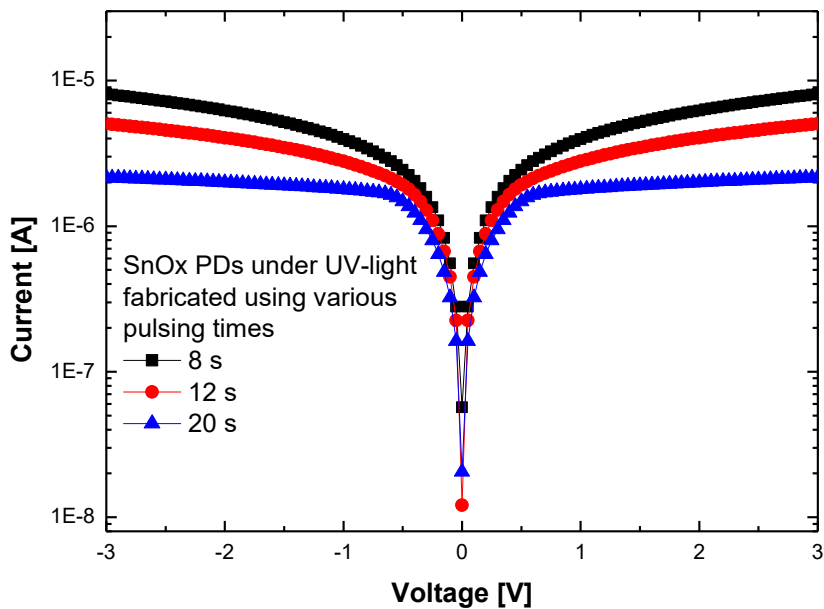


(c)

Figure.5



(a)



(b)

Figure.6

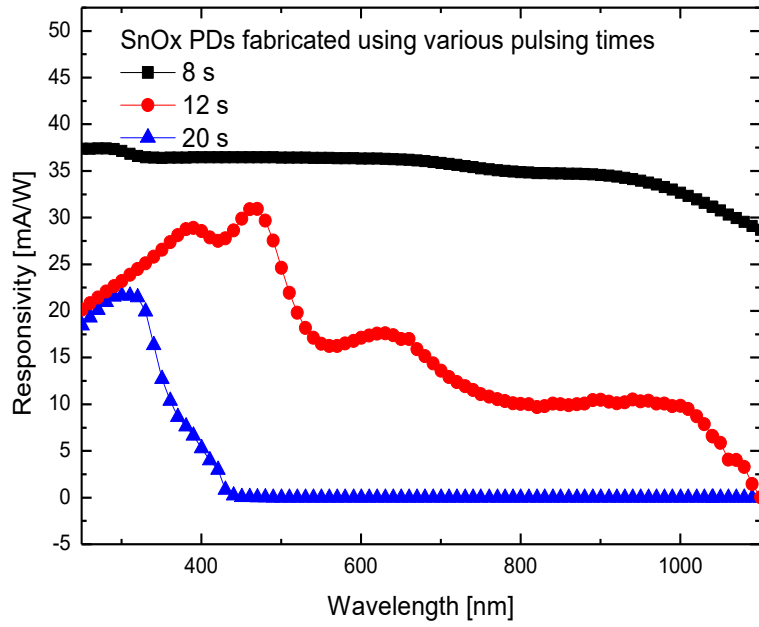


**Figure.7**

**Table.1**

UV-Vis-NIR PD structures	UV (300-365 nm)			Visible (green) (515-525 nm)			NIR (780-950 nm)			Ref.
	$I_{ON}/I_{OFF}$ (dB)	R (mA/W)	$D^*$ (Jones)	$I_{ON}/I_{OFF}$ (dB)	R (mA/W)	$D^*$ (Jones)	$I_{ON}/I_{OFF}$ (dB)	R (mA/W)	$D^*$ (Jones)	
Self-powered ZnO/NiO heterojunction	26	0.44	-	-	-	-	-	-	-	[35]
SnO <sub>2</sub> Microwire/CsPb Br <sub>3</sub> Heterojunction	35	0.35	1.6×10 <sup>10</sup>	35.5	0.46	1.2×10 <sup>10</sup>	-	-	-	[36]
n-SnOx/p-diamond heterojunction	8.1	0.04	-	-	-	-	-	-	-	[37]
SnO <sub>2</sub> -NiO heterojunction	22.3	0.14	8×10 <sup>8</sup>	-	0.04	-	-	-	-	[38]
SnOx/ZnO heterojunction	-	36.7	1.5×10 <sup>11</sup>	-	53.0	2×10 <sup>11</sup>	-	-	-	[39]
Ag/Si/ZnO/ITO heterojunction	-	0.72	2.2×10 <sup>9</sup>	-	79.9	2.5×10 <sup>10</sup>	-	17.9	2.9×10 <sup>9</sup>	[40]
ITO/Ag/ITO multilayer	30.5	0.05	1.2×10 <sup>10</sup>	-	-	-	-	-	-	[41]
ZnO NWs/PbS QDs	59	51	3.4×10 <sup>8</sup>	39	7.2	4.9×10 <sup>7</sup>	26.8	11	4.2×10 <sup>7</sup>	[42]
Elaborated Au/SnOx @ t <sub>ON</sub> = 8 s	26.1	36.45	1.1×10 <sup>11</sup>	26	36.41	1×10 <sup>11</sup>	25.6	34.7	9.5×10 <sup>10</sup>	This work
Elaborated Au/SnOx @ t <sub>ON</sub> = 12 s	30.1	25.1	1.3×10 <sup>11</sup>	28	19.8	1.1×10 <sup>11</sup>	21.1	9.2	4×10 <sup>10</sup>	This work
Elaborated Au/SnOx @ t <sub>ON</sub> = 20 s	55.3	21.8	5.8×10 <sup>11</sup>	-	-	-	-	-	-	This work